Scattering anisotropy-weighted mesoscopic imaging

Zhengbin Xu,[a] Ally-Khan Somani,[b] and Young L. Kim[a]
[a]Purdue University, Weldon School of Biomedical Engineering, 206 S. Martin Jischke Drive, West Lafayette, Indiana 47907
[b]Indiana University School of Medicine, Department of Dermatology, 550 N. University Boulevard, Indianapolis, Indiana 46202

Abstract. We report that when tissue images are formed via a small solid angle in the backward direction (i.e., back-directional gating), the image intensity is dominantly determined by tissue scattering anisotropy. Thus, this configuration allows for scattering anisotropy-weighted imaging that can provide an intrinsic contrast by capturing tissue structures and organizations. To demonstrate the immediate feasibility, we apply scattering anisotropy-weighted imaging to tissue blocks including basal-cell carcinomas as a pilot study. The main feature of our imaging approach is the high sensitivity to tumor locations and the simplicity for large-area visualization. We further envision that scattering anisotropy-weighted imaging could potentially be used to visualize tissue microenvironments in a mesoscopic (between microscopic and macroscopic) imaging setting. © *2012 Society of Photo-Optical Instrumentation Engineers (SPIE).* [DOI: 10.1117/1.JBO.17.9.090501]

Advances in bioimaging rely on the development of methods or probes that can provide unique imaging contrasts. Among those, the properties of light elastically scattered from tissue have shown the potential for the characterization of tissue structural alterations and the diagnosis of diseases. For example, numerous studies have shown that tissue morphological, structural, and organizational changes can play an important role in tumor initiation and progression in several types of cancer.[1,2] Recently, imaging methods that can quantify tissue microenvironments (e.g., collagen extracellular matrix) have been the objective of intensive investigation. In this respect, among several scattering properties, we hypothesize that scattering anisotropy in tissue could potentially serve as an imaging contrast. The anisotropy factor g, which is defined as the average cosine $\langle \cos \theta \rangle$ of the scattering angle θ, is a measure of the directionality of elastic light scattering. Thus, the arrangement of aligned or ordered microstructures dominantly attributes to this unique property. In other words, g can be used as a measure of the cellular and tissue organizations as an intrinsic imaging contrast.

Address all correspondence to: Young L. Kim, Purdue University, Weldon School of Biomedical Engineering, 206 S. Martin Jischke Drive, West Lafayette, Indiana 47907. Tel: 765-496-2445; Fax: 765-496-1459; E-mail: youngkim@purdue.edu

In this letter, we demonstrate that back-directional gated imaging allows g to dominantly attribute to the intensity of light backscattered from tissue, independent of scattering coefficients, and that the g-weighted imaging method can provide a novel contrast for tumors in a mesoscopic (i.e., between microscopic and macroscopic) imaging setup. In our previous studies,[3,4] we reported that back-directional gating can enhance contrast, resolution, imaging depth (~1 to 1.5 mm), and imaging area (~15 mm × 15 mm). In back-directional gating, a small aperture in the detection 4-focal length (4-f) lens system collects nearly exact backscattered light from tissue within a small angular cone of 2 to 5 deg. Unexpectedly from a Fourier optics standpoint, this configuration is highly beneficial to remove unwanted diffusive light because tissue is a highly anisotropic diffusive medium. Another key advantage of g-weighted imaging is a large imaging area, compared with conventional microscopy methods. When tumors are heterogeneous in a large tissue area (e.g., ~10 mm × 10 mm), examining a small area using microscopic techniques can fail to provide a representative or accurate assessment. In this study, we also show that the utilization of g will be useful for mesoscopic imaging.

To test how the light collected under back-directional gating is affected by the interplay between g and the scattering mean free pathlength ls, we first conducted a series of numerical experiments using optical ray-tracing combined with Monte Carlo simulations, by mimicking the detection configuration of our back-directional gated imaging system.[4,5] Briefly, a pencil beam was normally incident onto a bulk scattering medium and backscattered photons were collected through a 4-f lens system. An adjustable aperture in the 4-f lens system allowed us to vary the collection angle θ of the backscattered photons. In particular, we implemented two back-directional collection angles $\theta = 5$ deg and 25 deg that correspond to our back-directional gating and conventional imaging setups, respectively. A virtual detector was set at the conjugated plane to the surface of the scattering medium. The Henyey-Greenstein phase function was implemented in the Monte-Carlo simulations. We varied the anisotropy factor of the bulk medium $g = 0.6$ to 0.9 and the scattering mean free pathlength $ls = 50$ to 700 μm in the range of typical tissue optical properties. We maintained a minimal optical thickness of 70 in each simulation, which avoided the effect that the number of backscattered photons is strongly determined by a thin optical thickness. We launched 10 million photons and recorded the number of photons hitting the detector.

In Fig. 1, we plotted the total hits over ls at different g. When $\theta = 25$ deg [Fig. 1(a)], the number of collected photons depends both on g and ls. For example, as g and ls increase, the total hit of photons on the detector decreases, as expected. In this case, the signal is attributable both to g and ls. Surprisingly, when $\theta = 5$ deg [Fig. 1(b)], the number of collected photons, however, does not depend on ls for a given g. In other words, at a given ls, the total hit of backscattered photons is mainly determined by changes in g. These results support the idea that back-directional gating can allow us to utilize g as an imaging contrast. We note that this finding is also in good agreement with the Monte Carlo simulations on forward scattering through turbid media with different collection angles.[6] Importantly, as g increases, the difference in the signal level becomes more significant. A small change at a high level of g can produce a drastic change in the contrast. Given that most biological tissue is
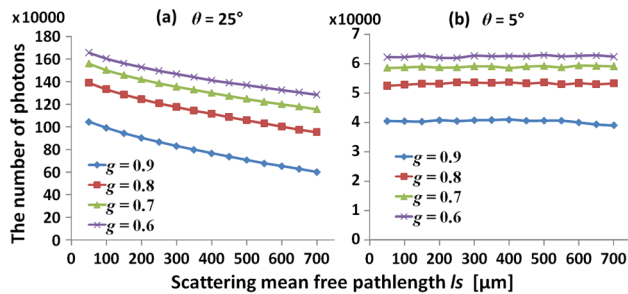
Fig. 1 Numerical experiments using optical ray-tracing combined with Monte-Carlo simulations. The number of photons detected by the virtual detector over different optical properties when the back-directional angle $\theta = 25$ deg (a) and $\theta = 5$ deg (b), corresponding to back-directional gating and conventional imaging setups, respectively. Surprisingly, when $\theta = 5$ deg, the number of collected photons does not depend on ls for a given g. Thus, the scattering intensity image obtained under back-directional gating can mainly be sensitive to changes in g.

highly anisotropic, this indicates the ability to visualize a subtle change in g induced by alterations in tissue structures and organizations. Thus, the scattering intensity or image obtained under back-directional gating is referred to as a g-weighted signal or image.

As a model system to test the feasibility of g as a novel imaging contrast, we used thick resected tissues of basal-cell carcinomas (BCCs) obtained from Mohs micrographic surgery, because it is well documented that BCCs involve degeneration and realignment of the extracellular matrix.[7–10] In this pilot study, we obtained four representative specimens with tumors that were confirmed histologically from adjacent slide sections. We imaged the fresh resected tissue blocks from the dermal side because residual tumors were included on the dermal side. The backscattering spectrum within $\lambda = 400 - 700$ nm at each (x, y) pixel was recorded using our back-directional gated spectroscopic imaging system.[4,5] Absorption of hemoglobin in the visible spectral range can potentially mask the scattering contrast from the anisotropic effect as reported in other studies.[11] Indeed, without removing the hemoglobin absorption, a low intensity can be attributable to both strong hemoglobin absorption and

high anisotropic property. To exclude the absorption from hemoglobin, we used a model comprised of power-law dependence on the wavelength λ for the scattering component and the Beer's law for the absorption of hemoglobin including a packaging effect correction.[12] After fitting each spectrum at each (x, λ) pixel to the model, we extracted the scattering contribution (i.e., power-law decay over λ) and generated a scattering intensity map deprived of the hemoglobin absorption (i.e., g-weighted image). We generated two g-weighted images by summing the intensity within $\lambda = 400 - 450$ nm and $\lambda = 650 - 700$ nm for each specimen after the nonuniformly distributed hemoglobin contribution is removed.

Figure 2 shows representative g-weighted images of four specimens (thickness $= 2 - 3$ mm) along with histology readings from the most adjacent thin section (thickness $= 5$ μm). Images on each row are from the same specimen (case 1: nodular infiltrative BCC; case 2: superficial nodular BCC; case 3: infiltrative BCC; and case 4: superficial nodular BCC). The first two columns [Fig. 2(a) and 2(b)] are pseudo-color images within the longer ($\lambda = 650 - 700$ nm) and shorter ($\lambda = 400 - 450$ nm) wavelength ranges, respectively. To obtain objective tumor contrasts accounting for specimen-to-specimen variations and to compare two different g-weighted images from the same specimen, we normalized the intensity of images to the same scale as shown in Fig. 2(a) and 2(b). In the third column [Fig. 2(c)], corresponding histology images of each specimen were generated by mosaicing approximately 20 microscopic images from the adjacent thin-slide section. BCCs were confirmed from individual histological readings and were circled on the mosaic image by the Mohs surgeon (A.K. Somani) who also served as a pathologist. In g-weighted images, the overall intensity within the tumors is lower than that of the surrounding tissue, suggesting that the localized BCCs have highly anisotropic properties.

Interestingly, the shorter wavelength g-weighted images [Fig. 2(b)] depict fine spatial patterns in greater details and display higher tumor-to-surrounding tissue contrasts. For example, the g-weighted image of case 1 shows that the tumor region has a much lower intensity than that of the surrounding tissue, yielding a sharper border. One of the possible reasons is that the
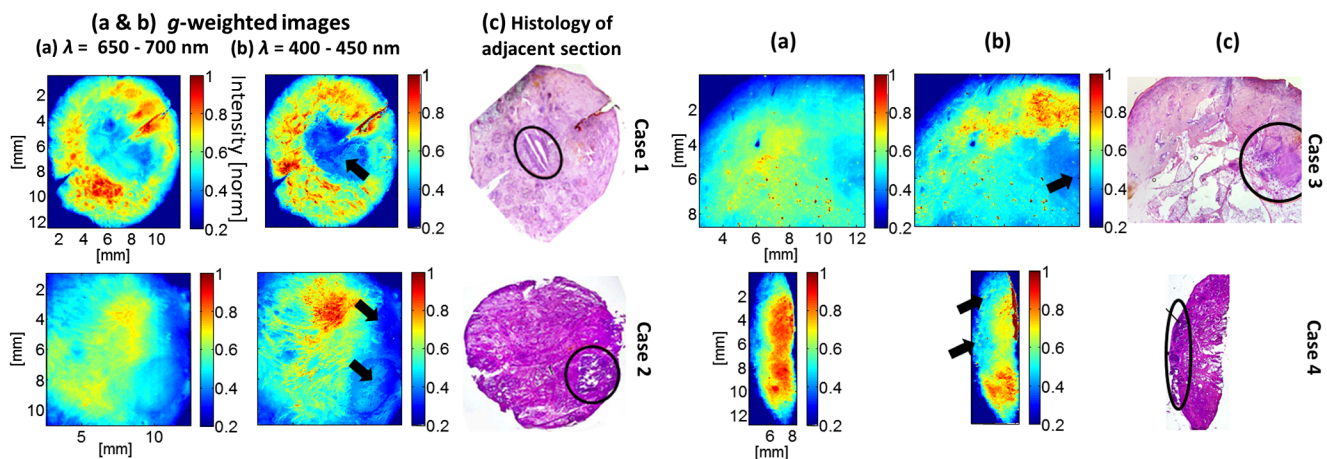
Fig. 2 Representative cases of resected thick tissue blocks (thickness = 2 to 3 mm) with BCCs. g-weighted images are generated by summing the intensity within $\lambda = 650$ to 700 nm (a) and $\lambda = 400$ to 450 nm (b). Overall, g-weighted images at the low wavelengths show enhanced contrasts between tumor and nontumor areas, because the scattering intensity decreases over the wavelength in tissue. (c) Histology from the most adjacent thin frozen section (thickness = 5 μm). Each histological image is generated by mosaicing ~20 low-resolution microscopy images and the locations of BCCs are circled. As indicated by the arrows, the larger tumor areas in the g-weighted images suggest that the residual tumors in the tissue blocks would be larger than those of the thin histological sections.

scattering intensity exponentially decays over the wavelength, which enhances the intensity at the lower wavelengths. In other words, at the lower wavelengths, the value of g-weighted image is significantly higher than at the longer wavelengths. In addition, a reduced optical thickness of the specimen at the longer wavelengths could potentially lead to more leakage to the transmitted light. Overall, g-weighted images at shorter wavelengths have advantages of depicting enhanced tumor contrasts as well as heterogeneous tissue organizations in details. We also note that the tumor areas in the g-weighted images are larger than the marked tumor regions in the histological images. For example, case 2 shows an additional low intensity area (arrows in Fig. 2) on the far right side of the specimen. Given a relatively deep imaging depth of back-directional gating ($\sim$1 to 1.5 mm),[4] the larger tumor area in the g-weighted image indicates that the residual tumor in the tissue block would be larger than that of the thin histological section. This is in part because the depth of g-weighted imaging is much deeper than the thin section of the histology slide.

A possible origin of this unique tumor contrast in g-weighted imaging is likely to link to changes in the extracellular matrix in the stromal tissue (e.g., collagen matrix remodeling and realignment), although changes in subcellular organelles (e.g., nuclear morphology) might minimally be attributable to g-weighted imaging. Indeed, several recent studies have showed that morphological and organizational alterations in the extracellular matrix occur in tumor initiation and progression in several types of cancer. For example, collagen fibers are often aligned and thickened during tumor progression (identified as tumor-associated collagen signatures) that is also contributed by carcinoma-associated fibroblasts. Microstructural alterations in the extracellular matrix have been shown in several types of cancer, including skin cancer, breast cancer, and ovarian cancer.[13] Such quantification has also been used to provide a biomarker of prognosis for breast cancer.[14] Thus, although further detailed investigation is required, the increase in g in the tumor areas can be understood in this regard. In particular, correlations of g-weighted images with microscopic images obtained from multiphoton or second harmonic generation microscopy will be highly valuable,[8–10,15] although a large number of microscopic images are required to cover a comparable imaging area to our method.

Our results from the numerical experiments and the pilot biological tests demonstrate that the back-directional gated imaging configuration allows g to be an imaging contrast for tissue architecture and organizations. Because images are formed by a small solid angle in the backward direction and biological tissue is highly anisotropic, the image intensity in back-directional gating is mainly determined by g, independent of ls, when the optical thickness is sufficiently thick. Using resected skin tissue specimens of BCCs, we further show the feasibility of g-weighted imaging to obtain an intrinsic tumor contrast in a relatively large area. Although the exact origin of the anisotropic effect warrants further investigation, we anticipate that this imaging method of utilizing scattering anisotropy could potentially provide a simple yet powerful contrast in mesoscopic imaging settings.

Acknowledgments

References

1. T. Stylianopoulos et al., "Diffusion anisotropy in collagen gels and tumors: the effect of fiber network orientation," *Biophys. J.* **99**(10), 3119–3128 (2010).

2. M. Allen and J. L. Jones, "Jekyll and Hyde: the role of the microenvironment on the progression of cancer," *J. Pathol.* **223**(2), 162–176 (2011).

3. Z. Xu, J. Liu, and Y. L. Kim, "Diffuse light suppression of back-directional gating imaging in high anisotropic media," *J. Biomed. Opt.* **14**(3), 030510 (2009).

4. Z. Xu et al., "Back-directional gated spectroscopic imaging for diffuse light suppression in high anisotropic media and its preclinical applications for microvascular imaging," *IEEE J. Sel. Topics Quantum Electron.* **16**(4), 815–823 (2010).

5. Z. Xu et al., "Spectroscopic visualization of nanoscale deformation in bone: interaction of light with partially disordered nanostructure," *J. Biomed. Opt.* **15**(6), 060503 (2010).

6. E. Berrocal et al., "Laser light scattering in turbid media part I: experimental and simulated results for the spatial intensity distribution," *Opt. Express* **15**(17), 10649–10665 (2007).

7. U. Bertheim et al., "The stromal reaction in basal cell carcinomas. A prerequisite for tumour progression and treatment strategy," *Br. J. Plast. Surg.* **57**(5), 429–439 (2004).

8. S. J. Lin et al., "Discrimination of basal cell carcinoma from normal dermal stroma by quantitative multiphoton imaging," *Opt. Lett.* **31**(18), 2756–2758 (2006).

9. R. Cicchi et al., "Multidimensional non-linear laser imaging of basal cell carcinoma," *Opt. Express* **15**(16), 10135–10148 (2007).

10. N. Vogler et al., "Multimodal imaging to study the morphochemistry of basal cell carcinoma," *J. Biophotonics* **3**(10–11), 728–736 (2010).

11. A. M. Laughney et al., "Automated classification of breast pathology using local measures of broadband reflectance," *J. Biomed. Opt.* **15**(6), 066019 (2010).

12. J. C. Finlay and T. H. Foster, "Effect of pigment packaging on diffuse reflectance spectroscopy of samples containing red blood cells," *Opt. Lett.* **29**(9), 965–967 (2004).

13. O. Nadiarnykh et al., "Alterations of the extracellular matrix in ovarian cancer studied by second harmonic generation imaging microscopy," *BMC Cancer* **10**(1), 94–107 (2010).

14. M. W. Conklin et al., "Aligned collagen is a prognostic signature for survival in human breast carcinoma," *Am. J. Pathol.* **178**(3), 1221–1232 (2011).

15. J. Xylas et al., "Intrinsic optical biomarkers associated with the invasive potential of tumor cells in engineered tissue models," *Biomed. Opt. Express* **1**(5), 1387–1400 (2010).